X-636-64-282

SLOPE DETECTION AS A METHOD OF DETERMINING THE PEAK POWER POINT OF SOLAR ARRAYS

BY

JOHN PAULKOVICH

OCTOBER 1964

NASA

GODDARD SPACE FLIGHT CENTER

GREENBELT, MD.

SLOPE DETECTION AS A METHOD OF DETERMINING THE PEAK POWER POINT OF SOLAR ARRAYS

By
John Paulkovich

Long term satellite missions have been primarily dependent on solar cells as a source of electrical power. The power generating capability of the solar cells used in the power supply are sensitive to hard particle irradiation, temperature and illumination. Typical voltage-current characteristics under differing conditions of temperature and irradiation are shown in figure 1. Figures 14 and 15 depict the effect of illumination on cell output. The maximum power generation capability for each cell is defined by the largest rectangle which can be inscribed under the I-E curve. It may be seen from figure 1 that:

1. The absolute values of maximum power varies quite drastically under differing conditions of temperature and irradiation.

2. The occurrence of maximum power varies quite drastically with voltage and current.

At present the power system designer attempts to anticipate the operating condition in space and then chooses an optimum operational voltage or current at which to operate. Once chosen this value usually remains fixed throughout spacecraft life. This approach has the following disadvantages:

1. In a radiation environment initial power is sacrificed so that at the end of mission operation will be at maximum power.

2. Variations in environment from what is expected can be disastrous for the power supply.

3. Interplanetary space probes would be forced to sacrifice considerable power initially in order to compensate for the difference in solar intensity and temperature at some later time in the flight.

The solution to these problems is an electronic sensing system that will allow continuous operation at maximum power no matter what the operating environment. This report contains the description of such a system along with the results of initial tests on a breadboard model.

To determine the feasibility of this method a graphical analysis was made of solar cells under the following conditions:

1. Non irradiated at -25°C
2. Non irradiated at 76°C
3. Irradiated (10^{16} e/cm^2) 77°C
4. Irradiated (10^{16} e/cm^2) -25°C
5. Solar angles of 0, 40°, and 60°.

Figure 1 illustrates the possible variations in the E-I curves due to temperatures and space radiation environment. From figure 1 it becomes apparent that it is impossible to select any one voltage, or current for that matter, that will be at the peak power point under all conditions.

The problems involved in obtaining maximum power from the solar cells lie in the present method of charging the batteries. The most common method is to place the solar cells, battery pack and shunt regulator in parallel. The shunt regulator clamps the solar cell and battery voltages when they reach a predetermined level. Therefore, the solar array voltage is maintained at some predetermined maximum voltage.

Again referring to figure 1, it can be seen that if a certain maximum voltage is selected which will operate under all conditions, it would probably be in the vicinity of .2 volts per cell. If operation is selected for peak power from curve "A" of figure 1, then if we refer to figure 5, we can select the optimum voltage. Figure 5 is a reproduction of curve "A", figure 1, with a superimposed power curve. This power curve ("B" of figure 5) indicates maximum power at approximately .215 volt. If the load is operating at .215 volt, then optimum power will be delivered to the load. But now, if we refer back to curve "C" of figure 1, we will find that at .215 volt less current is available and obviously less power. Figure 4 is a reproduction of 1-C along with the power curves. At .215 volt approximately 5.9 milliwatts of power would be delivered to the load, while actually 11.5 milliwatts are available.

Curves 1-B and 1-C are reproduced in figures 3 and 4 and the same conditions prevail. From the foregoing it becomes apparent that a method of determining the peak power point and operating in this region is of the utmost importance for utilizing maximum available energy.

The method to be discussed is based on operation at a fixed "slope" of the E-I characteristic curve. Figures 2, 3, 4, and 5 are reproductions of each of the individual curves of figure 1 with a super-imposed power curve. Also indicated are the peak power point, the 95% power points, and the tangent to the curve at these points. 95% was arbitrarily selected as the lowest desirable operating point. The tangent has the slope x/y, where volts is represented by x and amperes is represented by y. In analyzing figures 2 through 5 we can see that there is a range of slopes which is within 95% of the peak power point under all conditions. But there is also the solar angle to consider. Figure 6 indicates the effects of solar angle from 0° to 60°. Note the change in scales. The original plot was 10 cells in series, to maintain uniformity, the x scale numbers have been altered by 1/10. Figures 7, 8, and 9 are reproductions of figure 6 along with the slopes and also a super-imposed power curve. Figure 10 illustrates the range of slopes in each of the preceding graphs. From figure 10, it becomes apparent that if the slopes were held between 8.5 and 12.5, operation would be 95% of the peak power point or better under all conditions except the 60° solar angle. A slope of 12.5 on the 60° solar angle curve, figure 9, represents approximately 93% of the available peak power. As the solar angle exceeds 60°, the deviation from peak power will increase. The solar angle then sets the limits of operation and should not exceed 60° for this set of conditions.

Since we are interested in the slope, then a method of scanning this slope is necessary. Figure 11 illustrates a block diagram of a slope detector. The scanner applies an AC voltage signal across points A and B of a constant magnitude. This scanner must be insensitive to DC load currents and sensitive only to the slope x/y. A change of slope causes a change in reflected current to the slope indicator.

An operational circuit that will perform this function is illustrated in figure 12.

The voltage across A-B will be constant and represent x. The AC loading effect will be inversely proportional to the slope x/y and reflect a current through the transformer and appear as a voltage across R_1. This voltage is then compared to a reference voltage which represents the desired slope. The differential amplifier will balance at the desired slope and the meter will be either positive or negative above or below the desired slope. This voltage difference may be utilized to control the load or charging circuit.

A breadboard model was constructed (refer to figure 13) and tested. The differential amplifier or comparator was connected to a 100-0-100 microampere meter. R_1 was made adjustable for various slope selections. E-I plots using an x/y plotter and S51 solar paddles are shown in figures 14 through 16. The plots represent full light intensity, partially shaded solar cells, full paddle, 1/2 paddle and 1/4 paddle, as indicated.

In figure 14, E-I traces of full paddle, 1/2 paddle, and a shaded 1/2 paddle are illustrated. The slope detector was set to slopes of 30, 70, 100, and 150. These various points are also indicated in figure 14. A slope of 70 was selected as being the nearest to the peak power point although not necessarily optimum. The slope detector was then set to a slope of 70 for figures 15 and 16. The arrows indicate the point selected by the slope detector (meter balanced). The lines drawn tangent to the E-I plots are for a calculated slope of 70. The calculated slope and the slope selected by the slope detector coincide very nicely. The curves of figure 15 may be extreme conditions since they represent a power excursion of almost 10 to 1. Although the solar paddles are likely to have shadowing conditions, it is very unlikely that they would be shadowed by 90%. Under lesser shadowing conditions the slope could be optimized for operation nearer to the peak power point.

Figure 17 illustrates the slope detector combined with a pulse width modulated regulator. This method of power detection combined with a pulse width modulated regulator would certainly increase the charging power to the satellite battery pack. The pulse width regulator would act as a matching transformer between the solar cells and the battery pack, while the slope detector would be the impedance sensing device and control circuit for maintaining this optimum match.

ACKNOWLEDGMENTS

Brian T. Cunningham and Luther W. Slifer, for the use of the solar laboratory facilities that these experiments could be conducted.

REFERENCE

Brian T. Cunningham, Robert L. Sharp, and Luther W. Slifer, Jr., The Electrical Characteristics of Irradiated Silicon Solar Cells as a Function of Temperature, NASA-Goddard Space Flight Center, Greenbelt, Maryland, March 30, 1964.

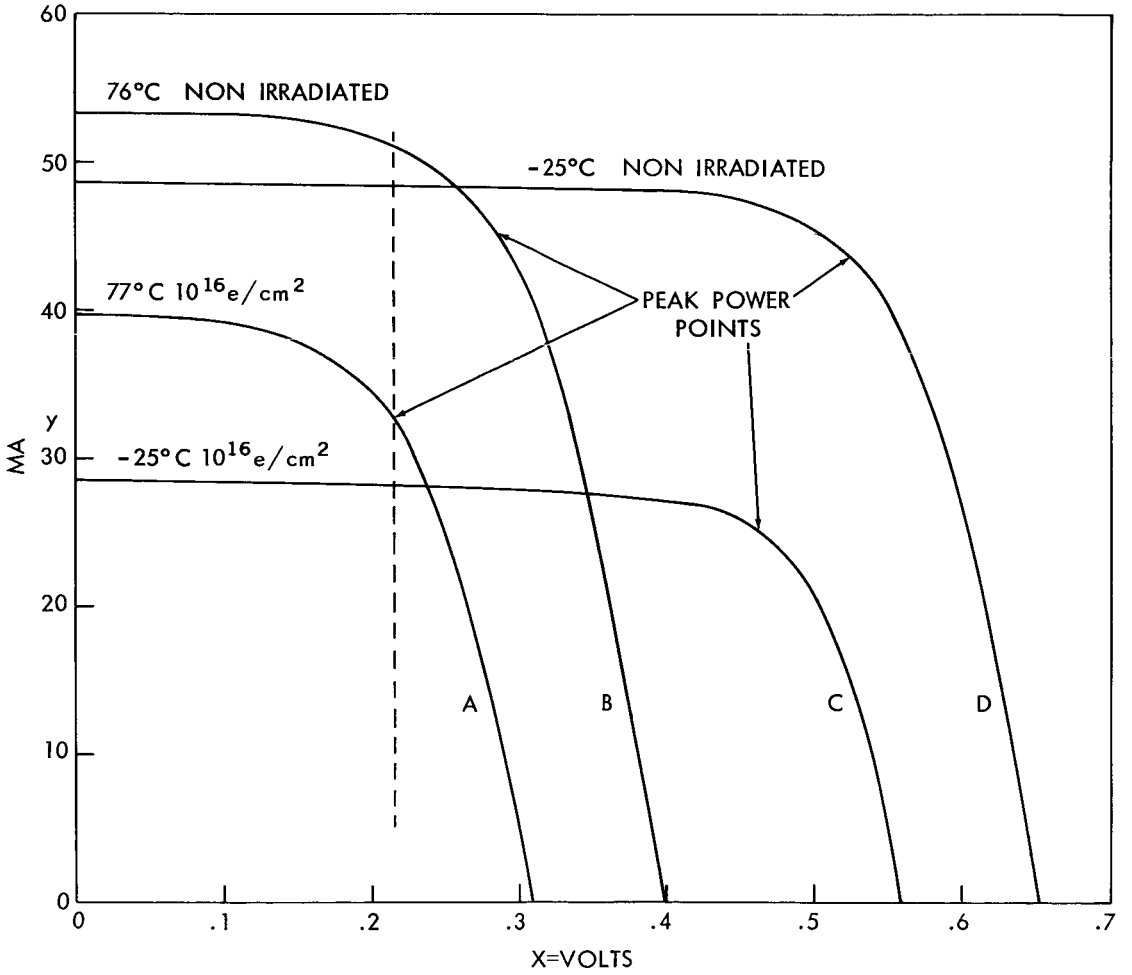

Figure 1—Typical N/P solar cell EI curves for various environmental conditions.

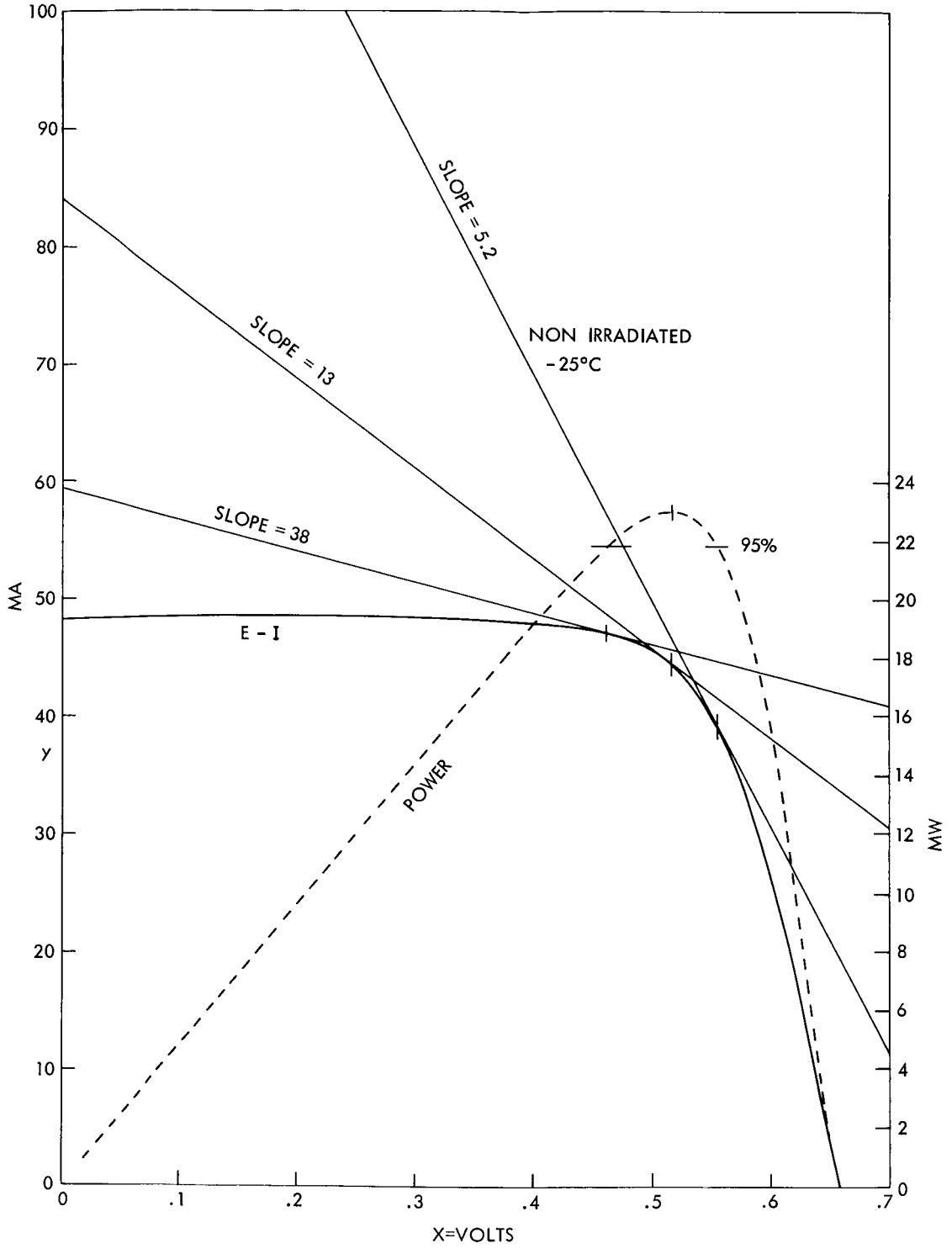

Figure 2—Graphical determination of optimum slope for maximum power coupling to detector for a non irriated solar cell at -25°C.

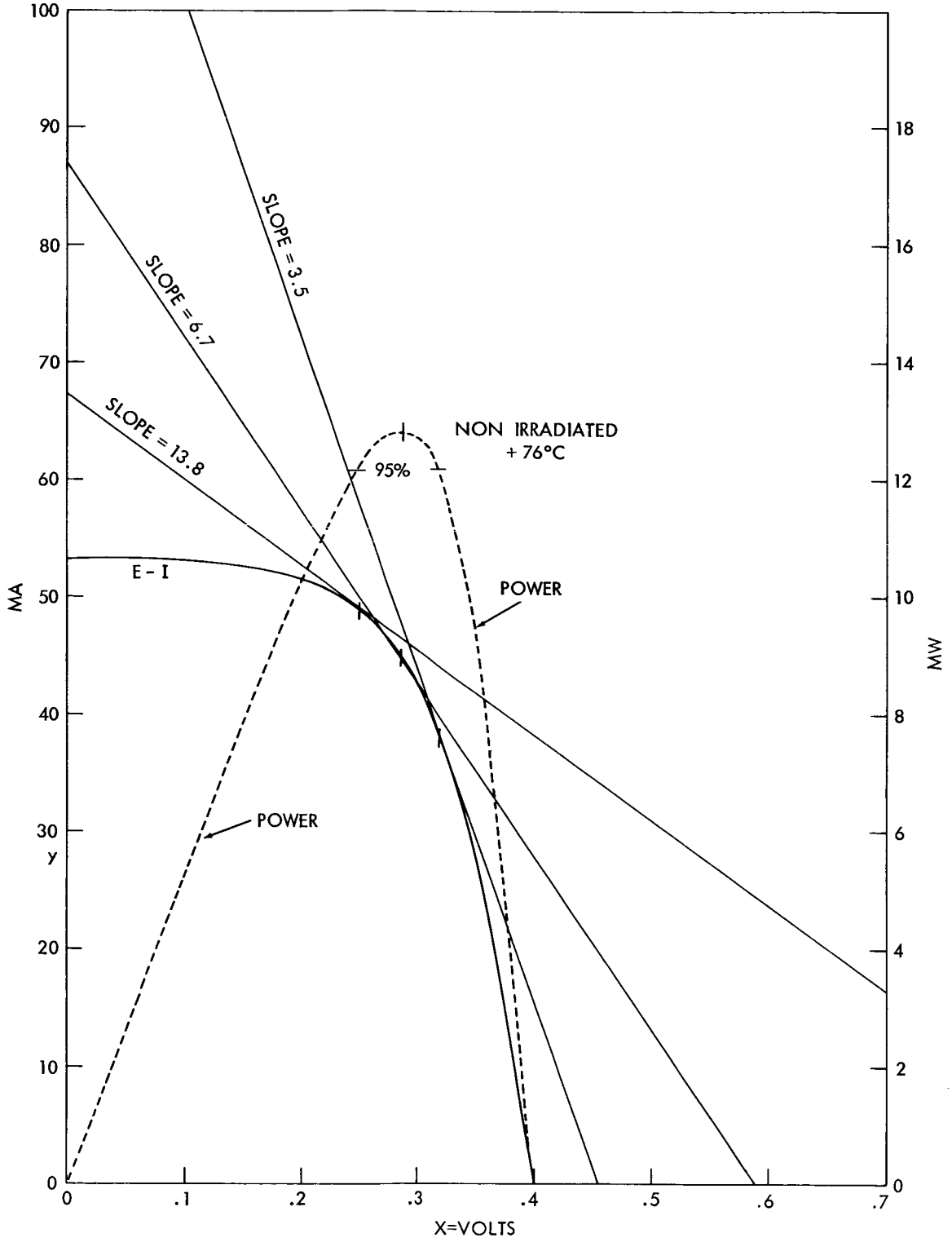

Figure 3—Graphical determination of optimum slope for maximum power coupling to detector for a non irriated solar cell at 76°C.

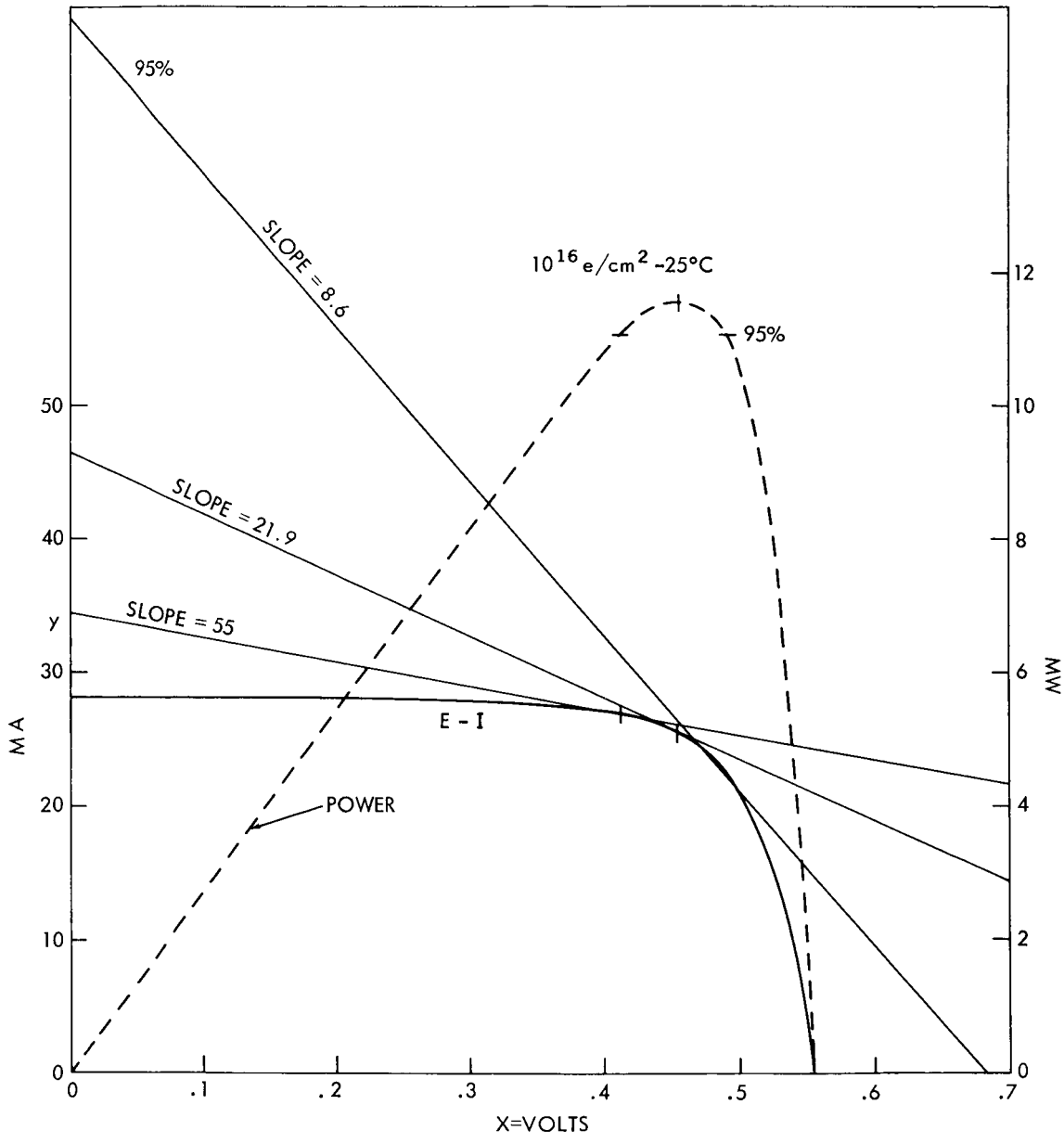

Figure 4—Graphical determination of optimum slope for maximum power coupling to detector for an irriated solar cell at -25°C.

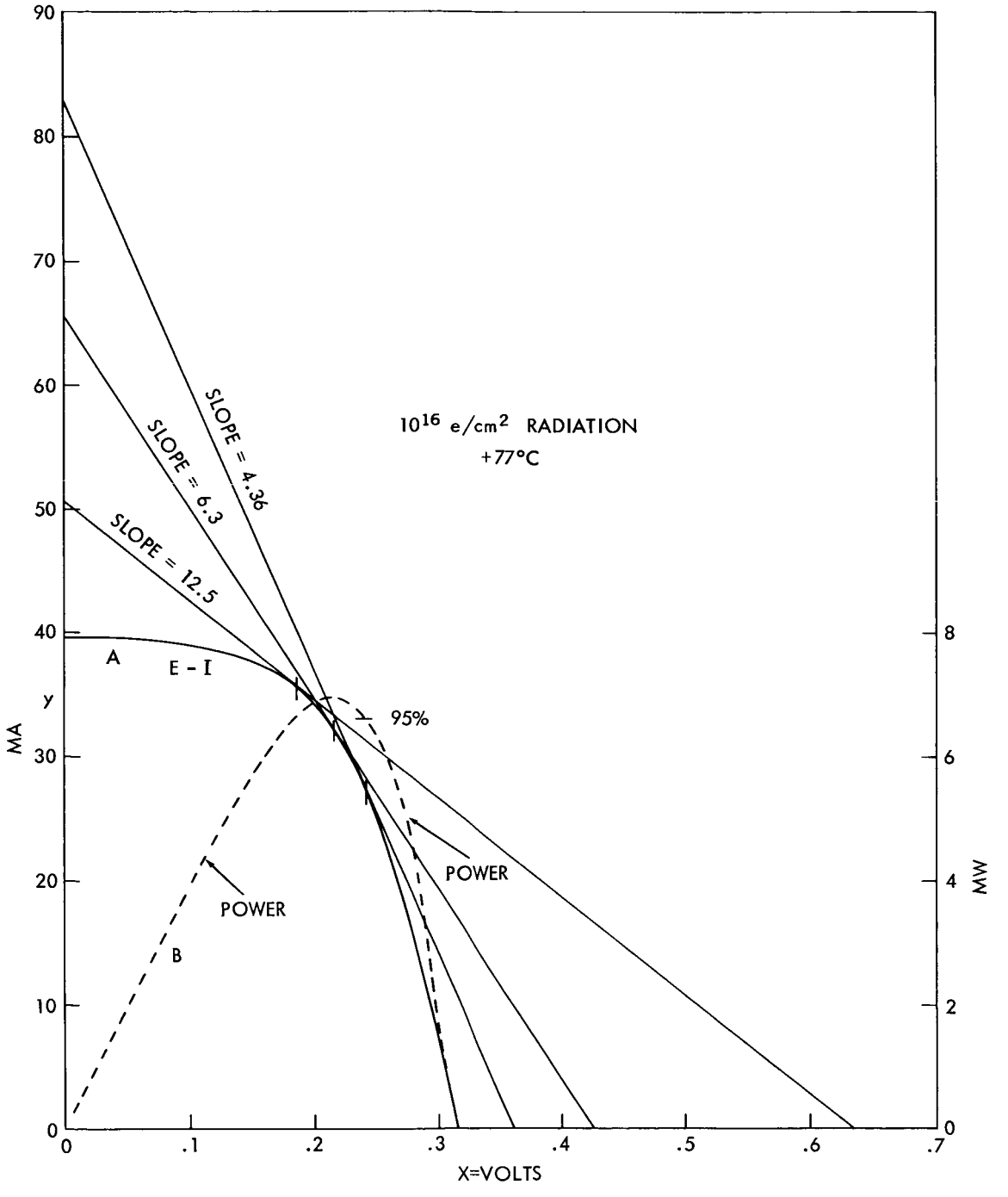

Figure 5—Graphical determination of optimum slope for maximum power coupling to detector for an irriated solar cell at 77°C.

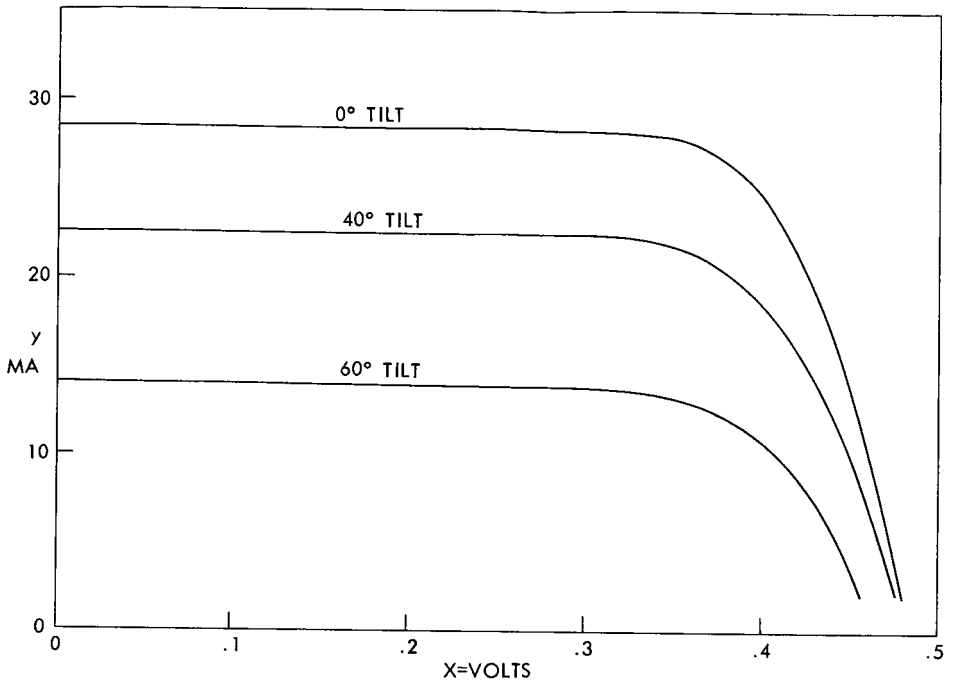

Figure 6—Typical solar cell EI curves vs angle of incidence.

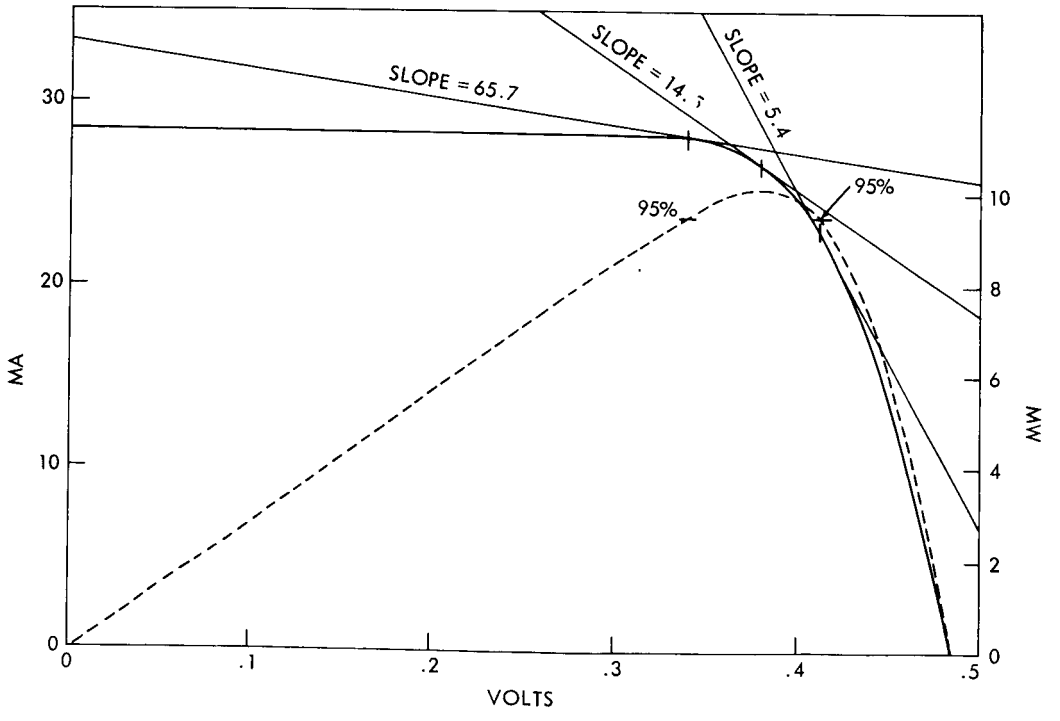

Figure 7—Typical solar cell EI curve at normal incidence.

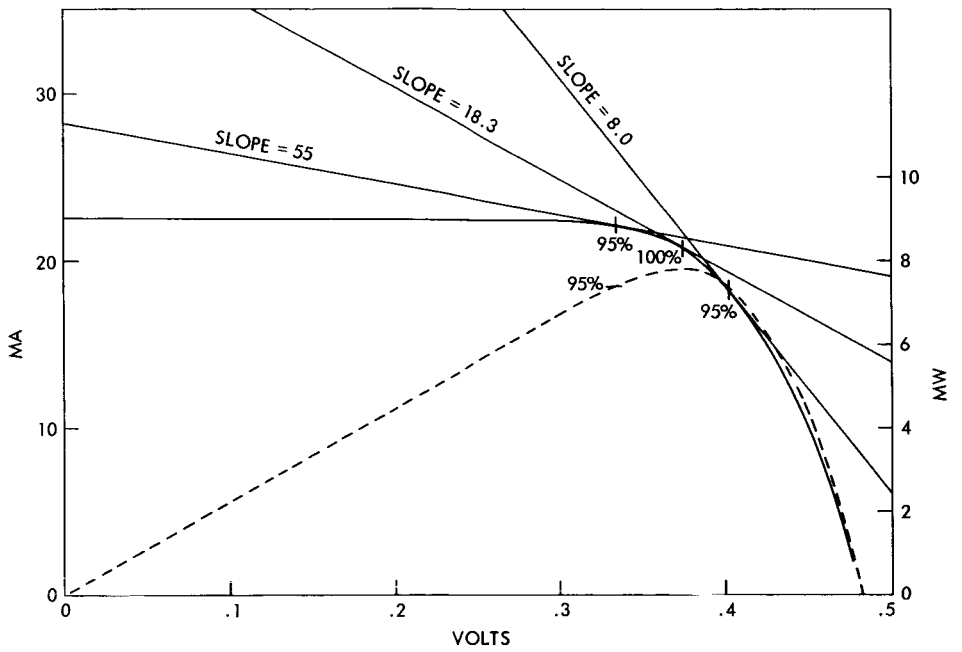

Figure 8—Typical solar cell EI curve at 40° tilt from normal incidence.

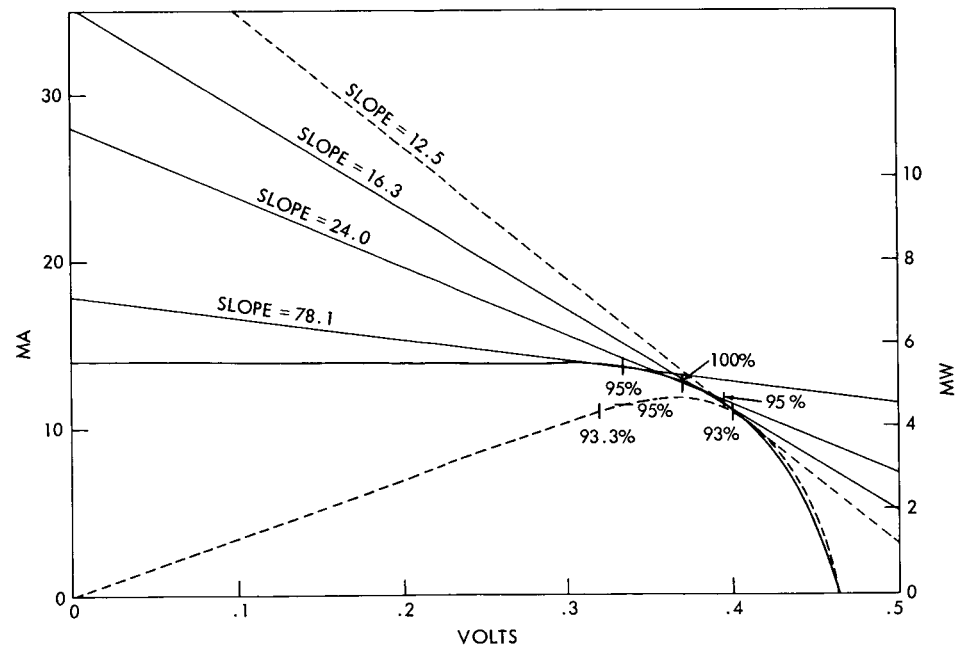

Figure 9—Typical solar cell EI curve at 60° tilt from normal incidence.

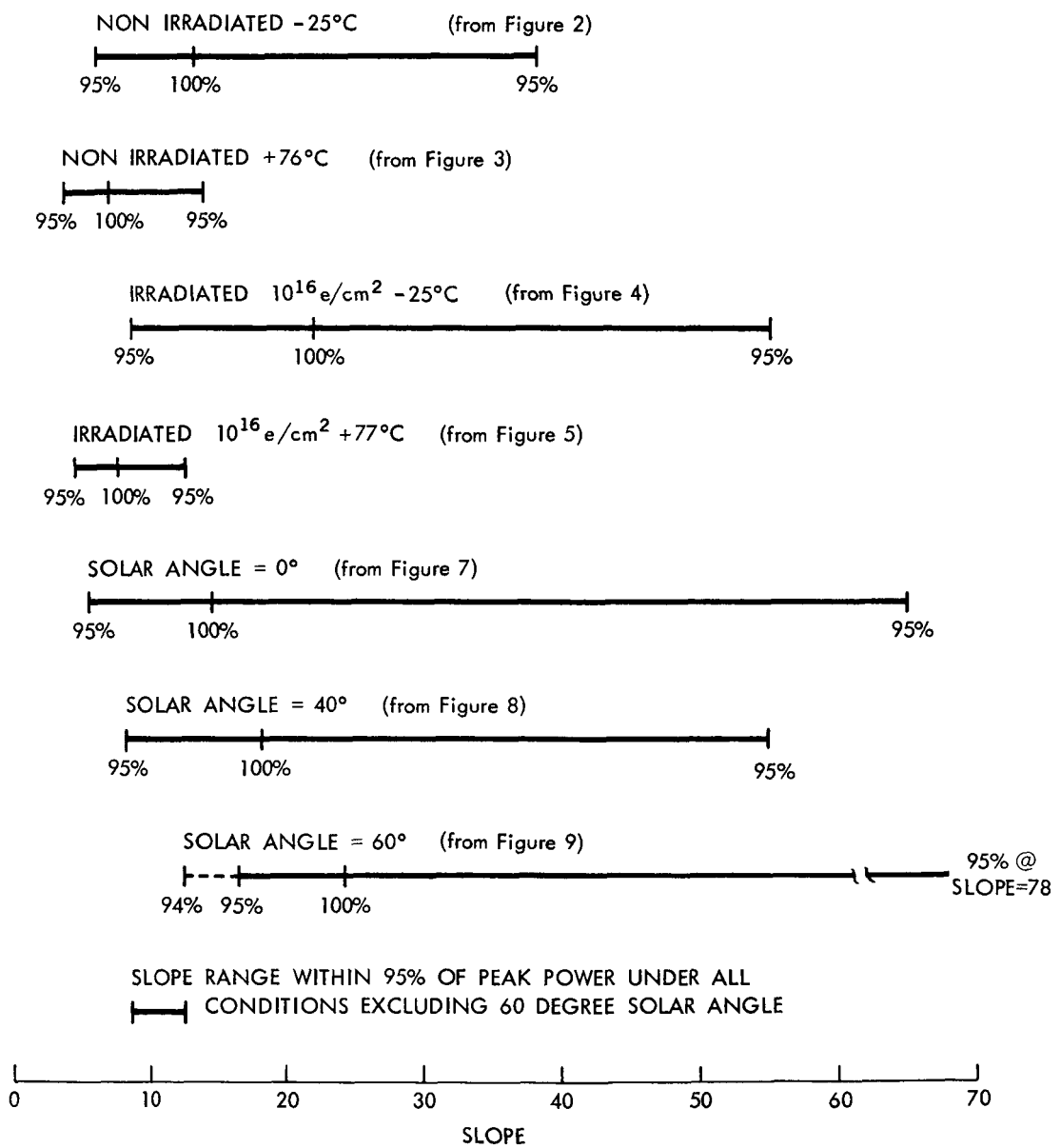

Figure 10—Compiled slope variation of Figures 2 through 9.

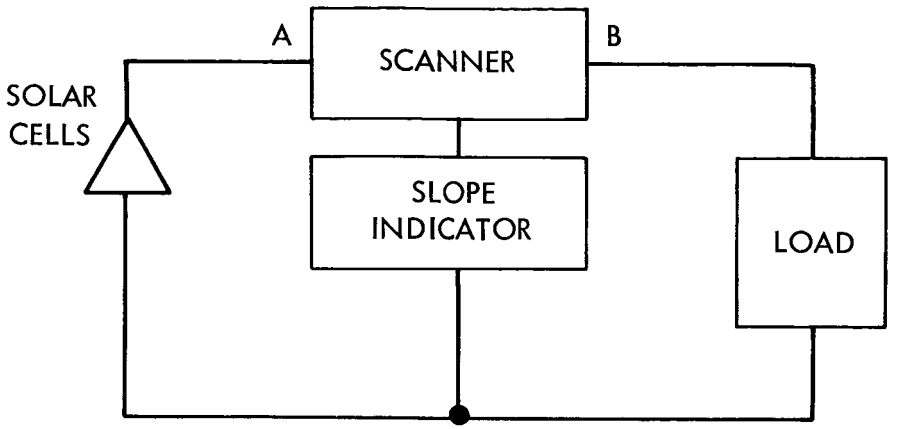

Figure 11—Block diagram of slope detector.

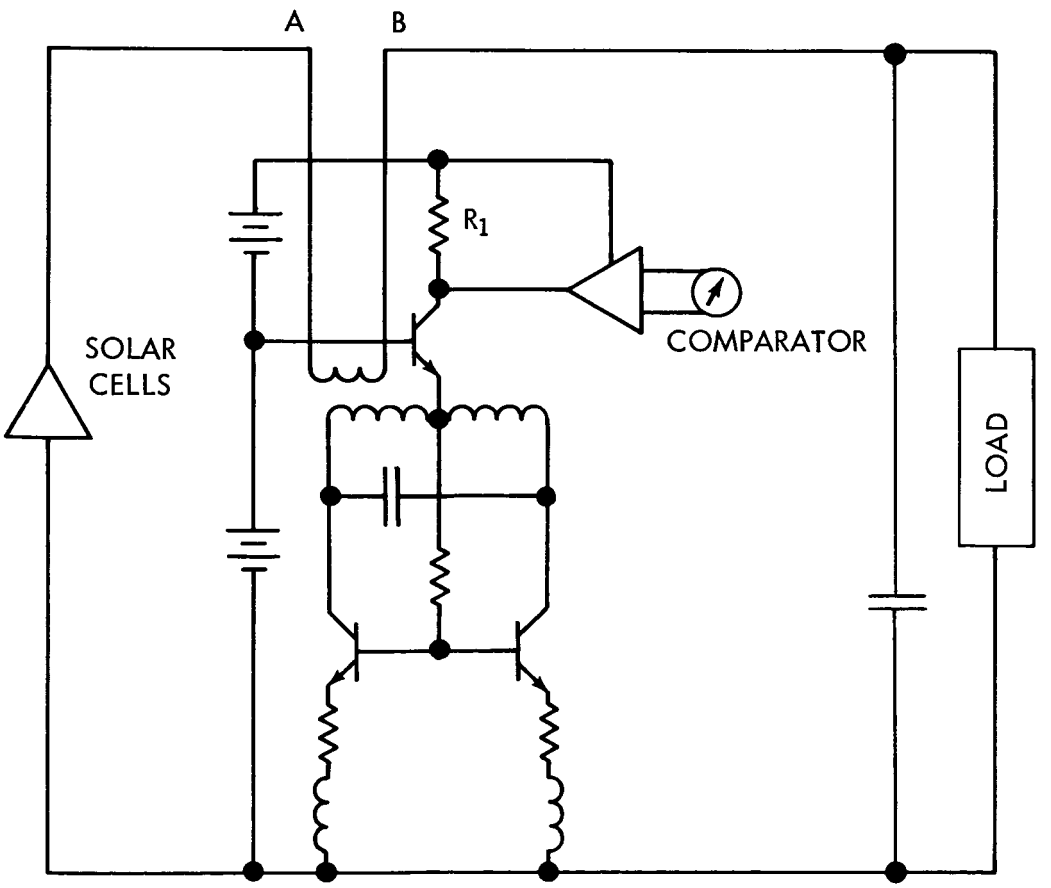

Figure 12—Basic circuit of slope detector.

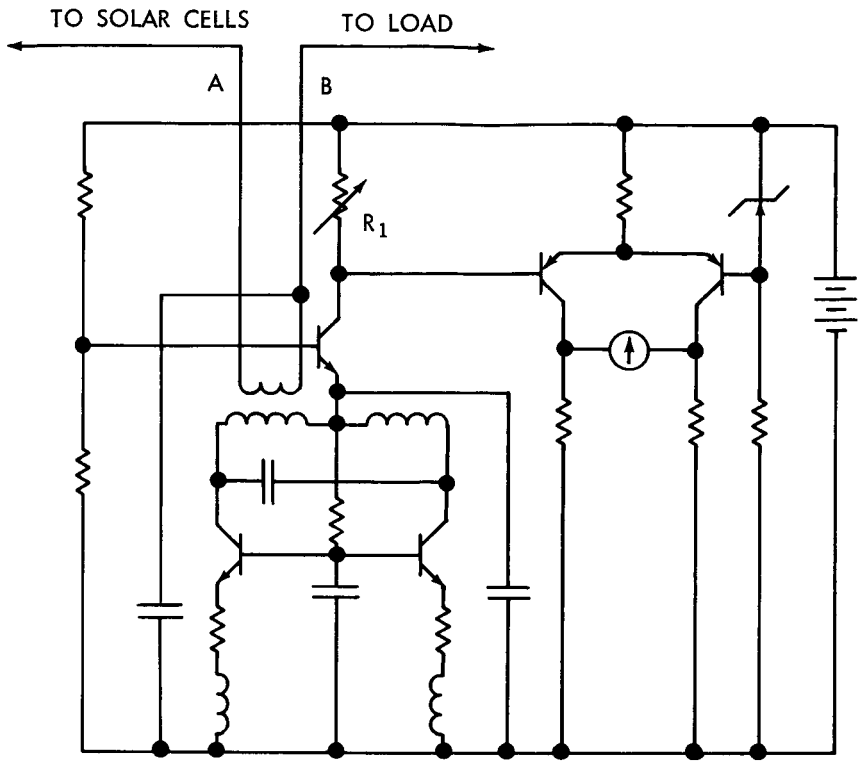

Figure 13—Schematic of the breadboard model of the slope detector.

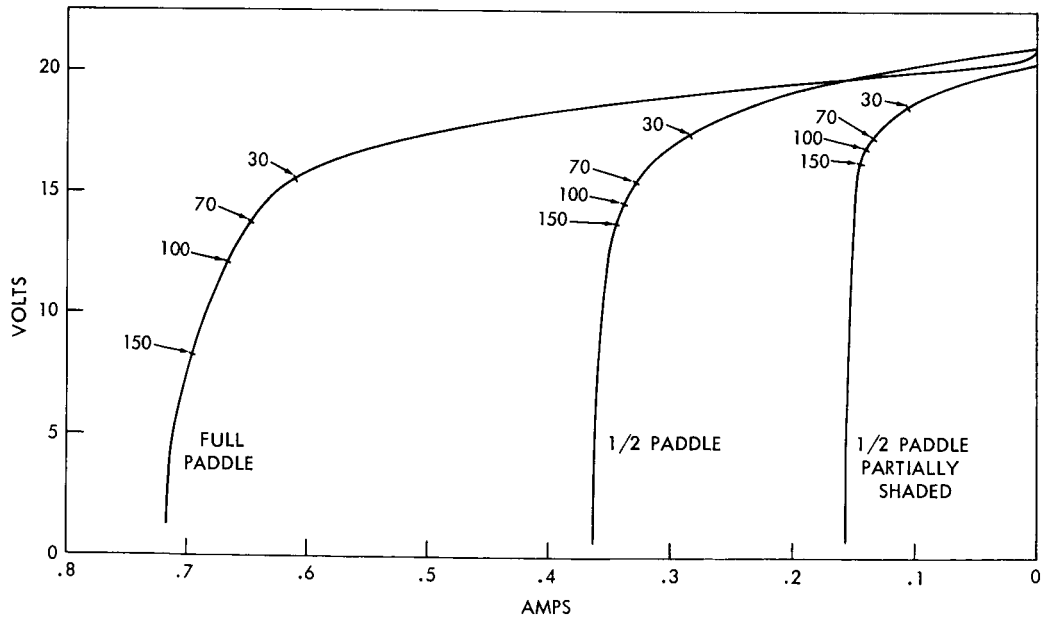

Figure 14—Solar paddle EI curves, slope detector set to 30, 70, 100 and 150.

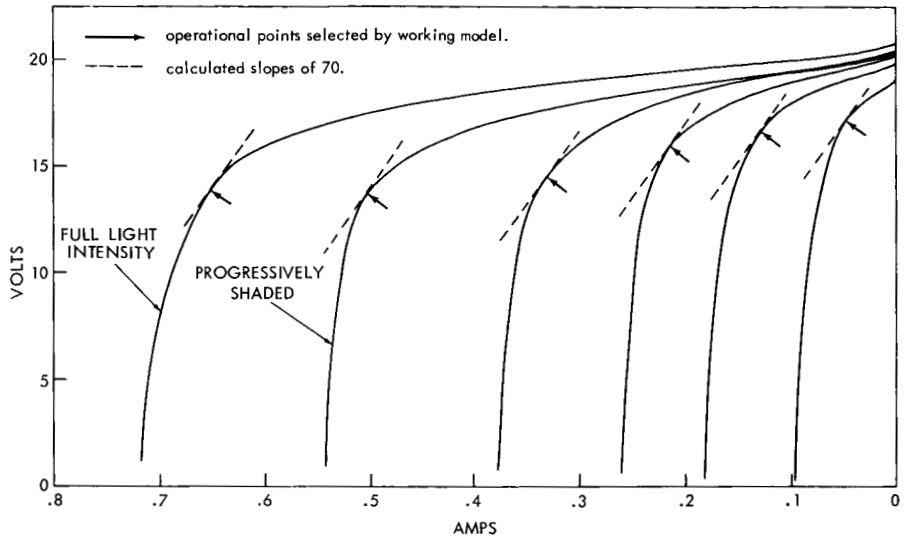

Figure 15—Solar paddle EI curves, slope detector set to 70.

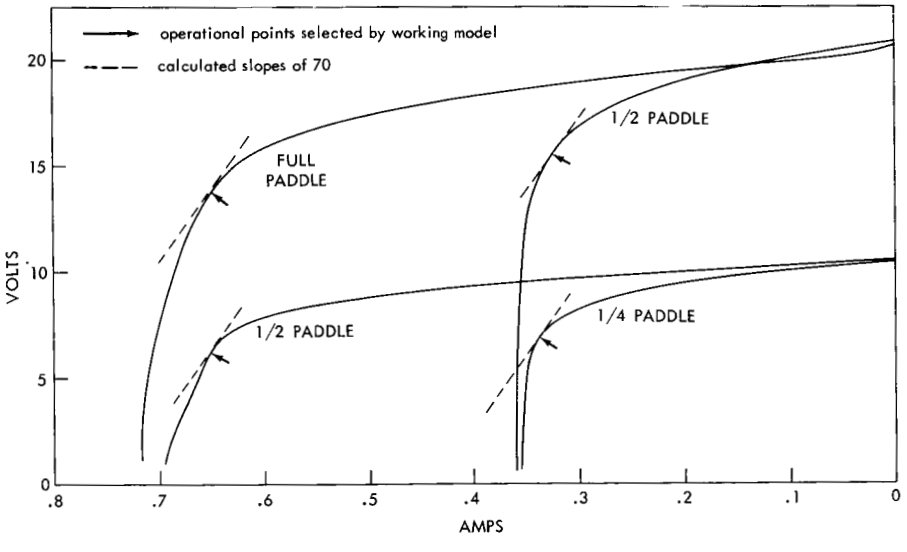

Figure 16—Solar paddle EI curves, slope detector set to 70.

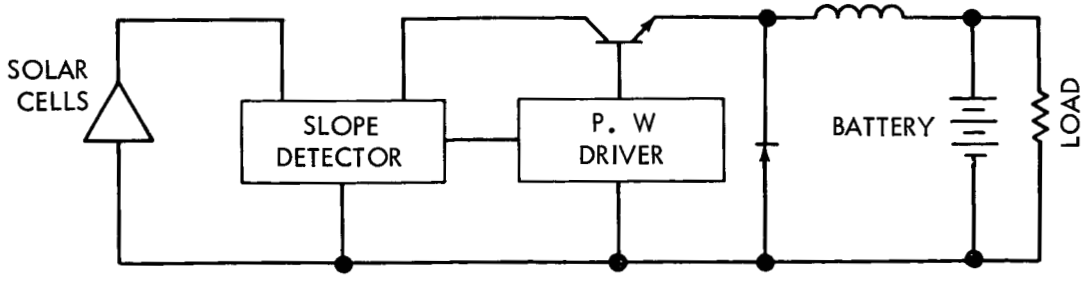

Figure 17—A block diagram of the slope detector controlling a pulse width modulated regulator for maintaining optimum matching between the load and the solar paddles.